

# A Structural Study of the Perovskite Series $\text{CaTi}_{1-2x}\text{Fe}_x\text{Nb}_x\text{O}_3$

Anton R. Chakhmouradian and Roger H. Mitchell

Department of Geology, Lakehead University, 955 Oliver Road, Thunder Bay, Ontario, Canada P7B 5E1

Received November 12, 1997; in revised form February 9, 1998; accepted February 17, 1998

An X-ray powder diffraction study of the series  $\text{CaTi}_{1-2x}\text{Fe}_x\text{Nb}_x\text{O}_3$  is presented. The series comprises orthorhombic perovskites ( $Pbnm$ ,  $a \approx b \approx \sqrt{2}a_p$ ,  $c \approx 2a_p$ ,  $Z=4$ ) in the range  $0 \leq x \leq 0.3$ , and monoclinic perovskites ( $P2_1/n$ ,  $a \approx b \approx \sqrt{2}a_p$ ,  $c \approx 2a_p$ ,  $\beta \neq 90^\circ$ ,  $Z=4$ ) in the range  $0.4 \leq x \leq 0.5$ . The structure of the orthorhombic members is derived from the cubic aristotype by octahedral rotation  $a^-a^-c^+$ . The structural distortion in the monoclinic members involves octahedral rotation and short-range cation ordering at the  $B$ -site ( $4c$  and  $4d$ ). In the series  $\text{CaTi}_{1-2x}\text{Fe}_x\text{Nb}_x\text{O}_3$ , the unit-cell parameters and degree of octahedral rotation increase with  $x$ . The  $[111]_p$  tilt angle increases from  $16.1^\circ$  in  $\text{CaTiO}_3$  to  $17.6$ – $18.9^\circ$  in  $\text{CaFe}_{1/2}\text{Nb}_{1/2}\text{O}_3$  (for the  $\text{NbO}_6$  and  $\text{FeO}_6$  octahedra, respectively). In contrast to previous studies, here the diffraction pattern of the end-member  $\text{CaFe}_{1/2}\text{Nb}_{1/2}\text{O}_3$  is interpreted to exhibit splitting of the  $hkl$  and  $h0l$  lines indicative of a monoclinic derivative of the  $\text{CaTiO}_3$ -type structure. © 1998 Academic Press

## INTRODUCTION

Among naturally occurring perovskite-type compounds, the mineral perovskite (ideally  $\text{CaTiO}_3$ ) is the most abundant in the Earth's crust. Compositional variations of naturally occurring perovskite-group minerals are important indicators of geochemical evolution in geological systems. Perovskite commonly contains significant amounts of Fe and Nb, thus forming a solid solution series with  $\text{CaFe}_{1/2}\text{Nb}_{1/2}\text{O}_3$  (1, 2). The maximum content of the  $\text{CaFe}_{1/2}\text{Nb}_{1/2}\text{O}_3$  end-member (up to 23.5 mol.%) calculated from the electron-microprobe analyses, is found in the mineral latrappite (2). The crystal structure of latrappite has been refined using the Rietveld method and shown to be orthorhombic and similar to that of  $\text{CaTiO}_3$  perovskite (2).

The structure of  $\text{CaTiO}_3$  perovskite has been studied extensively over the past five decades (3–9). This structure is derived from the aristotype by octahedral tilting about three four fold axes of the cubic subcell, and represents one of the fundamental perovskite hettotypes. The tilting results in orthorhombic symmetry of  $\text{CaTiO}_3$  (space group  $Pnma$  or  $Pbnm$ ). Most authors use the unconventional setting  $Pbnm$  with  $a \approx b \approx \sqrt{2}a_p$ ,  $c \approx 2a_p$  (5–8). In Glazer's (10) notation,

the octahedral tilting exhibited by  $\text{CaTiO}_3$  is written as  $a^-a^-c^+$ .

The compound  $\text{CaFe}_{1/2}\text{Nb}_{1/2}\text{O}_3$  has not been encountered in nature, but has been synthesized and shown to have the perovskite-type structure (11). Filip'ev and Fesenko (11) claim that  $\text{CaFe}_{1/2}\text{Nb}_{1/2}\text{O}_3$  has a monoclinically deformed perovskite cell, and exhibited no cation ordering at the  $B$ -site. Therefore, the actual symmetry of this perovskite was suggested to be orthorhombic with  $a \approx b \approx \sqrt{2}a_p$ ,  $c \approx a_p$ . The proposed monoclinic deformation of the perovskite cell implies a shear distortion such that the angle  $\beta$  between  $a_p$  and  $c_p$  is no longer  $90^\circ$ . The aluminous analogue of  $\text{CaFe}_{1/2}\text{Nb}_{1/2}\text{O}_3$  with the formula  $\text{CaAl}_{1/2}\text{Nb}_{1/2}\text{O}_3$  was suggested to have 1:1 cation ordering at the  $B$ -site, resulting in a doubling of the periodicity along  $c$  (11). It is noteworthy that among the complex oxides  $A^{2+}B^{3+}_{1/2}B^{5+}_{1/2}\text{O}_3$  ( $A^{2+} = \text{Ca, Sr, Ba, Pb}$ ;  $B^{3+} = \text{Al, In, Ga, Mn, Cr, Fe, Y, Bi, Ln}$ ;  $B^{5+} = \text{Nb, Ta, Sb}$ ), the majority exhibit partial or complete ordering of cations at the  $B$ -site (11–15). According to Fesenko *et al.* (12), the ordering is controlled by the difference in charge ( $\Delta q$ ) and radius ( $\Delta R_B = |R_{B(5+)} - R_{B(3+)}|/R_{B(5+)}$ ) of the cations. For the complex perovskites  $A^{2+}B^{3+}_{1/2}B^{5+}_{1/2}\text{O}_3$ ,  $\Delta R_B$  should exceed 0.09 for ordering to occur (12). High  $\Delta R_B$  (when  $B^{3+}$  approaches or exceeds  $A$  in radius) may result in the "inverse" perovskite structure (by analogy with the inverse spinel structure (11, 13)). For  $\text{Fe}^{3+}$ -bearing perovskites,  $\Delta R_B$  and thus the probability of cation ordering at the  $B$ -site, would depend on the spin state of  $\text{Fe}^{3+}$  (16).  $\Delta R_B$  calculated for  $\text{CaFe}_{1/2}\text{Nb}_{1/2}\text{O}_3$  using Shannon's ionic radii (16), is 0.14 for the low-spin  $\text{Fe}^{3+}$  and a mere 0.01 for the high-spin  $\text{Fe}^{3+}$ . This suggests that the ordering is more likely to occur when the  $\text{Fe}^{3+}$  cations are in the low-spin state. In the absence of long-range cation ordering, the perovskite structure may still exhibit reduction in symmetry due to short-range ordering, as has been demonstrated by Woodward (15) for  $\text{CaFe}_{1/2}\text{Ta}_{1/2}\text{O}_3$  (15).

The present work is a part of the comprehensive study of naturally occurring perovskite-type compounds and their synthetic analogues. The objective of the present work was to determine the structural characteristics of the series  $\text{CaTi}_{1-2x}\text{Fe}_x\text{Nb}_x\text{O}_3$ , with particular emphasis on the crystal chemistry of the end-member  $\text{CaFe}_{1/2}\text{Nb}_{1/2}\text{O}_3$  ( $x = 0.5$ ).

## EXPERIMENTAL

Compositions corresponding to the series  $\text{CaTi}_{1-2x}\text{Fe}_x\text{Nb}_x\text{O}_3$  were synthesized from stoichiometric amounts of  $\text{CaCO}_3$ ,  $\text{TiO}_2$ ,  $\text{Fe}_2\text{O}_3$ , and  $\text{Nb}_2\text{O}_5$  (high purity grade). The reagents dried at  $150^\circ\text{C}$  were mixed, ground in an agate mortar, and heated in air for 24 h at  $1100^\circ\text{C}$ . After regrinding, the samples were heated in air for 48 h at  $1300^\circ\text{C}$  and then rapidly cooled in air to room temperature. X-ray diffraction (XRD) powder patterns of the synthesis products were obtained on a Philips 3710 diffractometer ( $T = 20^\circ\text{C}$ ; radiation  $\text{CuK}\alpha$ ;  $2\theta$  range  $10^\circ$ – $145^\circ$ ;  $\Delta 2\theta$  step  $0.02^\circ$ ; time per step 2 s). The XRD patterns were analyzed by the Rietveld method using the FULLPROF program (17).

Compositions of samples were determined by X-ray energy-dispersion spectrometry (EDS) using a Hitachi 570 scanning electron microscope equipped with a LINK ISIS analytical system incorporating a Super ATW Light Element Detector (133 eV FWHM MnK). EDS spectra were acquired for 100 seconds (live time) with an accelerating voltage of 20 kV and beam current of 0.86 nA. The spectra were collected and processed with the LINK ISIS-SEM-QUANT software package. Well-characterized mineral standards were employed for the determination of Ca, Ti, Fe (perovskite), and Nb [Ioparite-(Ce)]. The accuracy of this method has been checked previously by wavelength-dispersion electron-microprobe analysis using an automated CAMECA SX-50 microprobe, following procedures described by Mitchell and Vladykin (18).

## RESULTS AND DISCUSSION

Complete solubility was observed between the end-members of the series  $\text{CaTi}_{1-2x}\text{Fe}_x\text{Nb}_x\text{O}_3$ . In most cases, the XRD patterns comprise only the diffraction lines of perovskite-type phases. For  $x = 0.1$  and  $0.2$ , the XRD patterns also include a weak diffraction line with  $d = 3.25 \text{ \AA}$ , which corresponds to the strongest reflection of rutile  $\text{TiO}_2$ . The intensity of this line does not exceed 1.6% of the strongest perovskite line (112). The SEM/EDS analysis also indicates the presence of minor rutile in the samples with  $x = 0.1$  and  $0.2$ .

The crystal structure of  $\text{CaTiO}_3$  at room temperature has been studied extensively and is well characterized (5–9). For the Rietveld refinement, we used data obtained by Sasaki *et al.* (5) as a starting structural model. In the present study, the unconventional space  $Pbnm$  was adopted instead of  $Pnma$ , as the former is more commonly applied to this perovskite hettotype by materials scientists. The results of the refinement for  $x = 0$  compare well with the previously published single-crystal and Rietveld structural data (Table 1). In the series  $\text{CaTi}_{1-2x}\text{Fe}_x\text{Nb}_x\text{O}_3$ , the orthorhombic distortion of the perovskite structure persists to the composition  $x = 0.3$ . The crystallographic characteristics of two

TABLE 1  
 $\text{CaTiO}_3$  ( $x = 0$ ): Comparison with Previously Published Structural Data

Characteristics	This study	Sasaki <i>et al.</i> (5)	Buttner and Maslen (6)	Liu and Lieberman (7)
$a, \text{ \AA}$	5.3814(1)	5.3796(1)	5.388(1)	5.3785(2)
$b, \text{ \AA}$	5.4418(1)	5.4423(3)	5.447(1)	5.4419(2)
$c, \text{ \AA}$	7.6409(2)	7.6401(5)	7.654(1)	7.6400(3)
Ca				
$x$	0.9937(7)	0.99324(7)	0.99371(7)	0.993(2)
$y$	0.0344(3)	0.03602(6)	0.03393(6)	0.033(1)
$z$	1/4	1/4	1/4	1/4
Ti				
$x$	0	0	0	0
$y$	1/2	1/2	1/2	1/2
$z$	0	0	0	0
O1				
$x$	0.068(1)	0.0714(3)	0.0707(3)	0.072(3)
$y$	0.485(1)	0.4838(2)	0.4842(2)	0.489(3)
$z$	1/4	1/4	1/4	1/4
O2				
$x$	0.712(1)	0.7108(2)	0.7109(1)	0.717(2)
$y$	0.2892(9)	0.2888(2)	0.2884(1)	0.284(2)
$z$	0.0402(8)	0.0371(1)	0.0370(1)	0.035(2)

orthorhombic members of the series ( $x = 0.1, 0.3$ ) are given in Table 2, and selected interatomic distances and bond angles in Table 3. As in  $\text{CaTiO}_3$ , the actual coordination number of the  $A$ -site cation for  $x = 0.1$ – $0.3$ , is eight ( $2 \times \text{O1} + 6 \times \text{O2}$ ), and the Ca polyhedron is a four-fold antiprism rather than a cubo-octahedron.

From Table 2 and Fig. 1, it is seen that the unit-cell parameters of perovskite increase with  $x$ . Given the significant difference between the ionic radii of  $\text{Ti}^{4+}$ , or  $\text{Nb}^{5+}$  and  $\text{Fe}^{3+}$  (16), it is expected that the distortion of the structure should also increase with  $x$ . As demonstrated by Zhao *et al.*

TABLE 2  
 $\text{CaTi}_{1-2x}\text{Fe}_x\text{Nb}_x\text{O}_3$ : Crystallographic Characteristics for  $x = 0.1$  and  $0.3$  (in *italic*)

Atom	Position	$x$	$y$	$z$	$B(\text{ \AA}^2)$
Ca	4c	0.994(1)	0.0340(4)	1/4	1.17(4)
		<i>0.992(1)</i>	<i>0.0386(5)</i>	—	<i>1.49(6)</i>
Ti (Fe, Nb)	4b	0	1/2	0	0.92(4)
		—	—	—	0.92(3)
O1	4c	0.071(1)	0.480(1)	1/4	0.5(2)
		<i>0.075(1)</i>	<i>0.481(1)</i>	—	<i>0.5(2)</i>
O2	8d	0.711(1)	0.291(1)	0.042(1)	1.6(2)
		<i>0.706(1)</i>	<i>0.290(1)</i>	<i>0.047(1)</i>	<i>1.4(2)</i>

Note. Final agreement factors and cell parameters for  $x = 0.1$ :  $R_p = 15.4$ ,  $R_{wp} = 22.2$ ,  $R_1 = 6.6$ ,  $\chi^2 = 1.62$ ,  $a = 5.3939(3)$ ,  $b = 5.4647(3)$ ,  $c = 7.6610(4) \text{ \AA}$ ; for  $x = 0.3$ :  $R_p = 14.3$ ,  $R_{wp} = 19.1$ ,  $R_1 = 6.6$ ,  $\chi^2 = 1.44$ ,  $a = 5.4217(5)$ ,  $b = 5.5079(5)$ ,  $c = 7.7077(7) \text{ \AA}$ .

TABLE 3  
 $\text{CaTi}_{1-2x}\text{Fe}_x\text{Nb}_x\text{O}_3$ : Selected Interatomic Distances (Å)  
 and Angles (°) for  $x = 0.1$  and  $0.3$

	0.1	0.3		0.1	0.3
Ca–O1	2.361	2.372	O1–B–O1	180.0	180.0
Ca–O1	2.475	2.477	$2 \times \text{O1–B–O2}$	87.8	87.4
Ca–O1	3.053	3.087	$2 \times \text{O1–B–O2}$	89.8	88.8
Ca–O1	3.065	3.105	$2 \times \text{O1–B–O2}$	90.2	91.2
$2 \times d$ Ca–O2	2.351	2.337	$2 \times \text{O1–B–O2}$	92.2	92.6
$2 \times d$ Ca–O2	2.612	2.598	$2 \times \text{O2–B–O2}$	89.0	89.1
$2 \times d$ Ca–O2	2.704	2.738	$2 \times \text{O2–B–O2}$	180.0	180.0
$2 \times d$ Ca–O2	3.270	3.349	$2 \times \text{O2–B–O2}$	91.0	90.9
$2 \times d$ B–O1	1.956	1.972	$2 \times \text{O2–B–O2}$	180.0	180.0
$2 \times d$ B–O2	1.959	1.981	B–O1–B	156.5	155.5
$2 \times d$ B–O2	1.982	2.005	B–O2–B	153.8	151.6

Note. B = Ti, Fe, Nb.

(19), the distortion of the orthorhombic  $Pbnm$  perovskites can be adequately described in terms of tilting of the  $BX_6$  octahedra about the  $[001]_p$  and  $[110]_p$  axes. In the literature, different symbols are used to denote the above octahedral rotations. This may result in confusion when the same symbol is applied to two different types of rotation (19,20). In the present work, we use the symbols suggested by Zhao *et al.* (19). The tilt  $\phi$  about  $[001]_p$  corresponds to a single in-phase rotation of the octahedra about the  $c$  axis of the orthorhombic ( $Pbnm$ ) cell. The tilt  $\theta$  about  $[110]_p$  combines two anti-phase rotations about  $[100]_p$  and  $[010]_p$  and can be viewed as an independent tilt about the  $b$  axis of the orthorhombic cell. The  $\phi$  and  $\theta$  rotations can be combined into a single tilt  $\Phi$  about the  $[111]_p$  axis (Fig. 2a). The

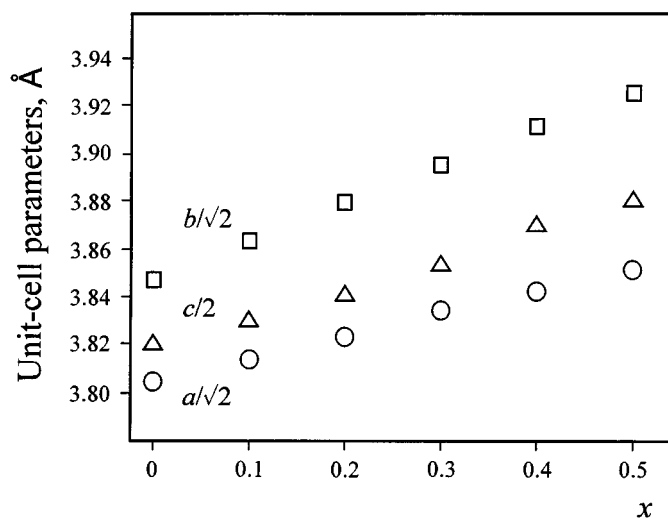


FIG. 1.  $\text{CaTi}_{1-2x}\text{Fe}_x\text{Nb}_x\text{O}_3$ : variation of the unit-cell parameters (reduced to pseudocubic) with the composition.

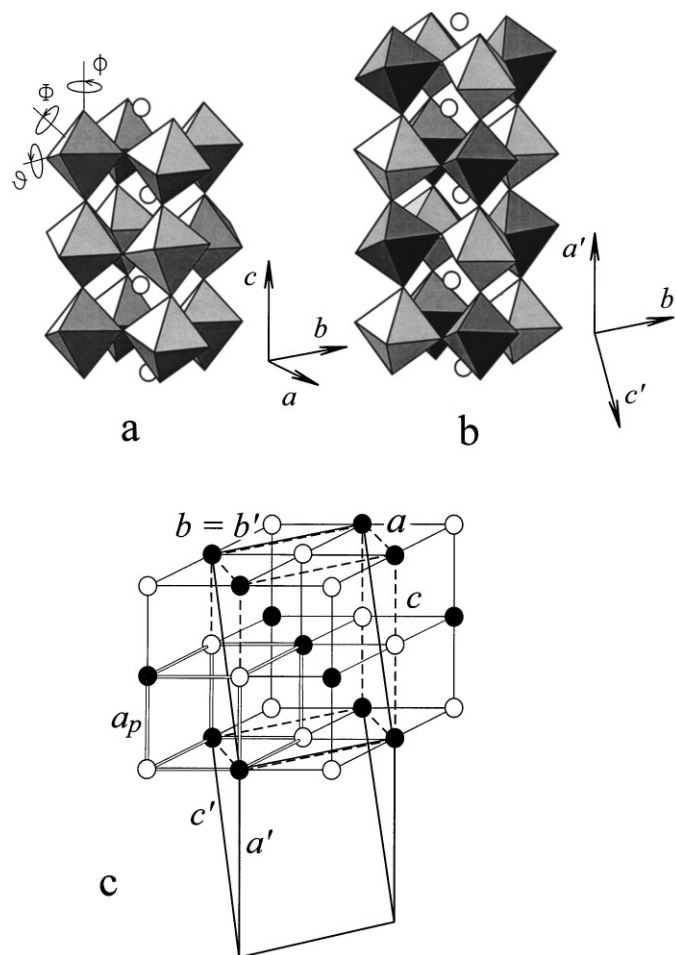


FIG. 2.  $\text{CaTi}_{1-2x}\text{Fe}_x\text{Nb}_x\text{O}_3$ : crystal structures and unit-cell relationships. (a) Orthorhombic structure of  $\text{CaTiO}_3$ ;  $\phi$ ,  $\theta$ , and  $\Phi$  denote octahedral tilting about  $[001]_p$ ,  $[110]_p$ , and  $[111]_p$ , respectively. (b) Monoclinic ordered structure of  $\text{CaFe}_{1/2}\text{Nb}_{1/2}\text{O}_3$ . Open circles represent  $\text{Ca}^{2+}$ , shaded polyhedra are  $\text{TiO}_6$  (a) and  $\text{FeO}_6$  and  $\text{NbO}_6$  (b). Crystallographic axes  $a$ ,  $b$ ,  $c$  correspond to the  $Pbnm$  or  $P2_1/n$  setting;  $a'$ ,  $b'$ , and  $c'$  to the  $P2_1/c$  setting. (c) Relationships between the pseudocubic subcell  $a_p \times a_p \times a_p$  corresponding to the aristotype  $Pm\bar{3}m$  (double line), cubic cell  $2a_p \times 2a_p \times 2a_p$  corresponding to the ordered untilted structure  $Fm\bar{3}m$  (thin solid line), and monoclinic cells  $a \times b \times c$  ( $P2_1/n$ , dashed line) and  $a' \times b' \times c'$  ( $P2_1/c$ , thick solid line) corresponding to the ordered tilted structure. Two types of B-cations are shown by open and solid circles.

tilt angles  $\phi$ ,  $\theta$ , and  $\Phi$  can be calculated using only the unit-cell parameters (19,20) or both unit-cell parameters and mean interatomic distance  $B\text{--}O$  (21). It is noteworthy that the tilt angles calculated using the latter method are consistently larger than those derived from the unit-cell dimensions alone (Fig. 3). However, regardless of the calculation method, in the compositional range  $0 \leq x \leq 0.3$ , the octahedral rotations smoothly increase with  $x$  (Fig. 3).

Peak splitting on the XRD pattern of  $\text{CaFe}_{1/2}\text{Nb}_{1/2}\text{O}_3$  ( $x = 0.5$ ) is essentially similar to that observed on the XRD pattern of  $\text{CaTiO}_3$ . For  $x = 0.5$ , most multiplets show better

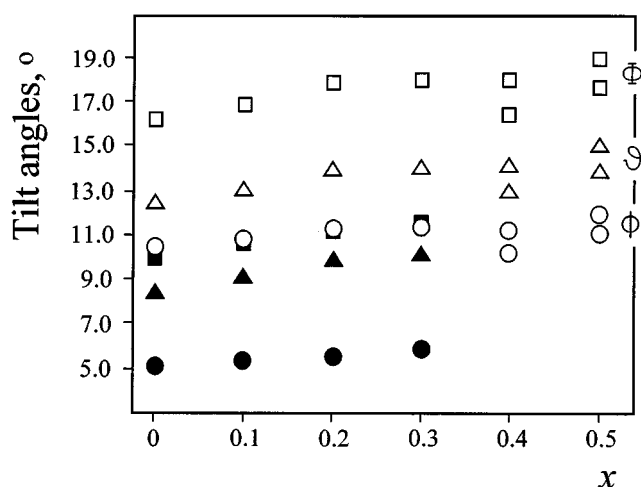


FIG. 3.  $\text{CaTi}_{1-2x}\text{Fe}_x\text{Nb}_x\text{O}_3$ : variation of the tilt angles with the composition. Solid symbols are tilt angles derived directly from the unit-cell parameters (19, 20), empty symbols are angles calculated from the unit-cell parameters and mean  $B\text{-O}$  distances (21).

resolution between the component peaks, indicating greater structural distortion compared to  $\text{CaTiO}_3$  (Table 4). On the XRD pattern of  $\text{CaFe}_{1/2}\text{Nb}_{1/2}\text{O}_3$ , the superstructure peaks  $h0l$  ( $h, l = \text{odd}$ ) are not observed, suggesting that there is no

TABLE 4  
X-ray Diffraction Data for  $\text{CaFe}_{1/2}\text{Nb}_{1/2}\text{O}_3$

$h$	$k$	$l$	$d$ (Å)	$I_{\text{obs}}$	$I_{\text{calc}}$	$h$	$k$	$l$	$d$ (Å)	$I_{\text{obs}}$	$I_{\text{calc}}$
1	1	0	3.89	54	53	1	2	3	1.790	1	1
0	0	2	3.88	23	23	2	1	-3	1.779	2	1
1	1	1	3.48	2	2	1	3	0	1.754	10	11
1	1	-1	3.48	3	2	2	2	2	1.740	5	4
0	2	0	2.778	48	50	2	2	-2	1.740	7	6
1	1	2	2.750	87	87	1	1	4	1.738	6	6
1	1	-2	2.750	100	100	1	1	-4	1.738	6	5
2	0	0	2.727	46	48	3	1	0	1.727	5	5
0	2	1	2.616	1	1	1	3	1	1.711	3	3
1	2	0	2.475	1	1	1	3	-1	1.711	3	3
2	1	0	2.448	2	2	1	3	2	1.598	17	16
1	2	1	2.358	2	2	1	3	-2	1.598	16	15
1	0	-3	2.339	6	6	0	2	4	1.592	23	22
2	1	1	2.334	3	3	2	0	4	1.582	13	13
2	1	-1	2.334	1	1	2	0	-4	1.582	10	10
1	1	3	2.156	3	3	3	1	2	1.579	22	21
1	1	-3	2.156	1	1	3	1	-2	1.578	24	23
1	2	2	2.087	1	1	1	3	3	1.452	1	1
1	2	-2	2.087	2	1	1	3	-3	1.452	1	1
2	1	2	2.070	1	1	0	4	0	1.389	8	7
2	2	0	1.946	70	67	2	2	4	1.375	16	16
0	0	4	1.942	35	34	2	2	-4	1.374	14	14
0	2	3	1.894	3	2	0	4	1	1.367	1	1
2	2	1	1.887	1	1	4	0	0	1.363	8	7
2	2	-1	1.887	2	1	3	2	-3	1.311	1	1

Note. Diffraction lines with  $I_{\text{obs}} < 1$  are omitted.

long-range ordering between  $\text{Fe}^{3+}$  and  $\text{Nb}^{5+}$ . However, the  $hkl$  and  $h0l$  lines are broadened, reduced in intensity, and flattened at the tip. This indicates further splitting of these lines into  $hkl + hk-l$  and  $h0l + h0-l$  components, and suggests a monoclinic distortion of the crystal structure. An orthorhombic-to-monoclinic reduction in symmetry without long-range ordering of the  $B$ -site cations has been described for  $\text{CaFe}_{1/2}\text{Ta}_{1/2}\text{O}_3$  and  $\text{CaMn}_{1/2}\text{Ta}_{1/2}\text{O}_3$  by Woodward (15). In this study, we tried both possible structural models, orthorhombic and monoclinic. A monoclinic unit-cell derived from the parental orthorhombic cell ( $Pbnm$  or  $Pnma$ ) by 1:1 cation ordering at the  $B$ -site corresponds to the space group  $P2_1/n$  ( $a \approx b \approx \sqrt{2}a_p$ ,  $c \approx 2a_p$ ,  $\beta \neq 90^\circ$ ) (22, 23).

As in the case of  $\text{CaFe}_{1/2}\text{Ta}_{1/2}\text{O}_3$  and  $\text{CaMn}_{1/2}\text{Ta}_{1/2}\text{O}_3$  (15), the refinement using the space group  $P2_1/n$  achieves better fit between the calculated and observed patterns than the refinement based on the orthorhombic  $Pbnm$  model. The reduction in symmetry may result from short-range ordering at the  $B$ -site due to the charge difference between  $\text{Fe}^{3+}$  and  $\text{Nb}^{5+}$ , rather than difference in ionic radii. The Mössbauer data on some synthetic (24) and naturally occurring Fe-bearing perovskites (C. McCammon, personal communication, 1997) are consistent with the high-spin state of  $\text{Fe}^{3+}$ . As noted above, high-spin  $\text{Fe}^{3+}$  and  $\text{Nb}^{5+}$  are similar in ionic radii (16).

Figure 4 illustrates good agreement between the calculated and observed patterns for  $x = 0.5$  and the space group  $P2_1/n$ . The crystallographic characteristics of  $\text{CaFe}_{1/2}\text{Nb}_{1/2}\text{O}_3$  are given in Table 5. The site occupancy refined by the Rietveld method supports the chosen structural model and indicates some degree of ordering between  $\text{Fe}^{3+}$  and  $\text{Nb}^{5+}$  at the  $4c$  and  $4d$  sites (Table 5). Selected interatomic distances and bond angles for  $x = 0.5$  (Table 6) demonstrate that the two types of octahedra are slightly different in size, and that the true coordination number of Ca is eight.

The structure of the ordered perovskite  $\text{CaFe}_{1/2}\text{Nb}_{1/2}\text{O}_3$  is compared with that of  $\text{CaTiO}_3$  in Figs. 2a and 2b. In  $\text{CaFe}_{1/2}\text{Nb}_{1/2}\text{O}_3$ , the  $\text{FeO}_6$  and  $\text{NbO}_6$  octahedra alternate along the  $x$ ,  $y$ , and  $z$  axes of the pseudocubic subcell. In the absence of octahedral rotation, the space group of such an ordered structure would be  $Fm\bar{3}m$  (Fig. 2c). As in the case of the orthorhombic  $\text{CaTiO}_3$ -type perovskites, the tilt angles  $\phi$ ,  $\theta$ , and  $\Phi$  can be used to characterize the distortion of the structure in  $\text{CaFe}_{1/2}\text{Nb}_{1/2}\text{O}_3$ . In contrast to the orthorhombic perovskites, the tilt angles cannot be derived directly from the unit-cell dimensions because the  $\beta$  angle is no longer  $90^\circ$ . Therefore, for  $\text{CaFe}_{1/2}\text{Nb}_{1/2}\text{O}_3$  we used the equations given by Groen *et al.* (21). The tilt angles were calculated from the unit-cell parameters assuming regularity of the octahedra, and compared to the tilt angles derived from the atomic coordinates. The values obtained by two different methods are in a good agreement with each other

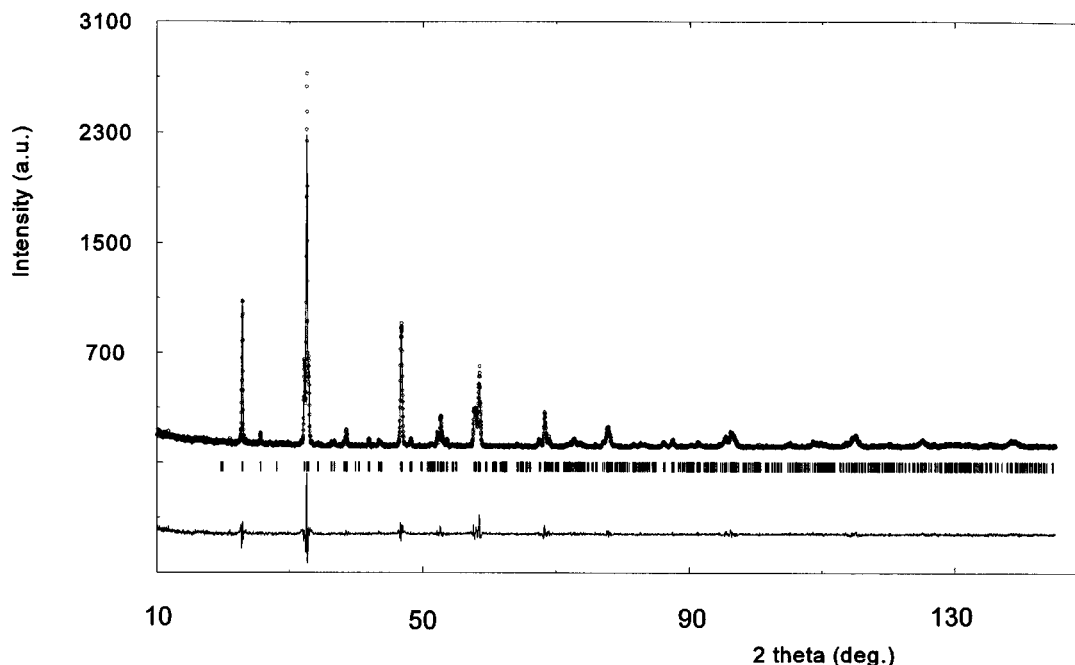


FIG. 4. Calculated (line) and observed (dots) XRD patterns and difference spectrum for  $x = 0.5$ . For the agreement factors see Table 5.

(Table 6). The XRD powder pattern of the perovskite with  $x = 0.4$  can be successfully refined using both orthorhombic and monoclinic structural models. Because the  $hkl$  and  $h0l$  diffraction lines on the XRD pattern appear split, we have favored the monoclinic model.

The unit-cell parameters of the monoclinic members of the series  $\text{CaTi}_{1-2x}\text{Fe}_x\text{Nb}_x\text{O}_3$  are compared with those of the orthorhombic members in Table 7 and Fig. 1. Variation of the tilt angles with composition is shown on Fig. 3. (Note

TABLE 5  
 $\text{CaTi}_{1-2x}\text{Fe}_x\text{Nb}_x\text{O}_3$ : Crystallographic Characteristics for  
 $x = 0.5$

Atom	Position	Site occupancy	$x$	$y$	$z$	$B$ ( $\text{\AA}^2$ )
Ca	4e	1	0.507(1)	0.5438(6)	0.254(1)	1.26(6)
Fe1	4c	0.33(7)	0	1/2	0	0.75(4)
Fe2	4d	0.17(7)	1/2	0	0	0.75(4)
Nb2	4d	0.33(7)	1/2	0	0	0.75(4)
Nb1	4c	0.17(7)	0	1/2	0	0.75(4)
O1	4e	1	0.200(4)	0.224(4)	-0.057(3)	0.7(6)
O2	4e	1	0.292(4)	0.684(4)	-0.033(3)	1.0(7)
O3	4e	1	0.427(2)	0.978(2)	0.256(2)	0.6(3)

Note. Final agreement factors:  $R_p = 14.6$ ,  $R_{wp} = 19.0$ ;  $R_1 = 6.4$ ;  $\chi^2 = 1.63$ ; cell parameters in the space group  $P2_1/n$ :  $a = 5.4480(4)$ ,  $b = 5.5517(4)$ ,  $c = 7.7612(5)$   $\text{\AA}$ ,  $\beta = 90.11(2)^\circ$ ; cell parameters in the space group  $P2_1/c$ :  $a = 7.7612(5)$ ,  $b = 5.5517(4)$ ,  $c = 9.474(3)$   $\text{\AA}$ ,  $\beta = 144.2(3)^\circ$ .  $B$  factors are kept at the same values for all  $B$ -site cations.

TABLE 6  
Selected Interatomic Distances ( $\text{\AA}$ ), Bond Angles ( $^\circ$ ),  
and Tilt Angles ( $^\circ$ ) for  $\text{CaFe}_{1/2}\text{Nb}_{1/2}\text{O}_3$  ( $x = 0.5$ )

Interatomic Distances and Bond Angles					
Ca-O1	2.336	$2 \times d$ Fe-O1	1.934	O2-Fe-O3	90.2
Ca-O1	2.560	$2 \times d$ Fe-O2	1.910	O2-Fe-O3	89.8
Ca-O1	2.797	$2 \times d$ Fe-O3	1.940	O3-Fe-O3	180.0
Ca-O1	3.431	$2 \times d$ Nb-O1	2.099	O1-Nb-O1	180.0
Ca-O2	2.396	$2 \times d$ Nb-O2	2.102	O1-Nb-O2	87.3
Ca-O2	2.634	$2 \times d$ Nb-O3	2.030	O1-Nb-O2	92.7
Ca-O2	2.721	O1-Fe-O1	180.0	O1-Nb-O3	85.0
Ca-O2	3.369	O1-Fe-O2	85.7	O1-Nb-O3	95.0
Ca-O3	2.389	O1-Fe-O2	94.3	O2-Nb-O2	180.0
Ca-O3	2.451	O1-Fe-O3	86.5	O2-Nb-O3	87.9
Ca-O3	3.110	O1-Fe-O3	93.5	O2-Nb-O3	92.1
Ca-O3	3.170	O2-Fe-O2	180.0	O3-Nb-O3	180.0

Tilt Angles <sup>a</sup>			
Derived from unit-cell parameters		Derived from atomic coordinates	
$\phi$ (Fe)	11.9	$\phi$ (Fe)	10.0
$\phi$ (Nb)	11.0	$\phi$ (Nb)	10.9
$\theta$ (Fe)	14.9	$\theta$ (Fe)	12.4
$\theta$ (Nb)	13.8	$\theta$ (Nb)	11.9
$\Phi$ (Fe)	18.9	$\Phi$ (Fe)	15.9
$\Phi$ (Nb)	17.6	$\Phi$ (Nb)	16.1

<sup>a</sup>Tilt angles calculated from the equations given by Groen *et al.* (21). The tilt  $\phi$  corresponds to rotation of the octahedra about  $[001]_p$ ,  $\theta$  to rotation about  $[110]_p$ , and  $\Phi$  to octahedral tilting about  $[111]_p$ .

**TABLE 7**  
 **$\text{CaTi}_{1-2x}\text{Fe}_x\text{Nb}_x\text{O}_3$ : Variation of Unit-cell Parameters (Å)**  
**and Angles (°)**

$x$	$a$	$b$	$c$	$\beta$
	Orthorhombic ( $Pbnm$ )			
0	5.3814(1)	5.4418(1)	7.6409(2)	90
0.1	5.3939(3)	5.4647(3)	7.6610(4)	90
0.2	5.4066(4)	5.4871(5)	7.6814(6)	90
0.3	5.4217(5)	5.5079(5)	7.7077(7)	90
	Monoclinic ( $P2_1/n$ )			
0.4	5.4358(5)	5.5342(5)	7.7414(5)	90.20(3)
0.5	5.4480(4)	5.5517(4)	7.7612(5)	90.11(2)

that the monoclinic members have different tilt angles for the two types of octahedra). From Figs. 1 and 3, it is obvious that the unit-cell dimensions and tilting of the octahedra correlate positively with  $x$ . The increase in tilt angles with increasing Fe and Nb contents presumably results from the structural tension created by difference in charge and radii between these two elements and Ti.

### CONCLUSIONS

The present work demonstrates complete solubility in the perovskite series  $\text{CaTi}_{1-2x}\text{Fe}_x\text{Nb}_x\text{O}_3$ . In the compositional range  $0 \leq x \leq 0.3$ , the XRD powder patterns show splitting of diffraction lines typical of the orthorhombic  $\text{CaTiO}_3$ -type perovskites. In the range  $0.4 \leq x \leq 0.5$ , the  $hkl$  and  $h0l$  diffraction lines are broadened and reduced in intensity, indicating a further reduction of symmetry to monoclinic. This distortion results from short-range ordering of  $\text{Fe}^{3+}$  and  $\text{Nb}^{5+}$  between the  $4c$  and  $4d$  sites. In the series  $\text{CaTi}_{1-2x}\text{Fe}_x\text{Nb}_x\text{O}_3$ , the unit-cell parameters and degree of octahedral tilting (measured in rotation angles  $\phi$ ,  $\theta$ , and  $\Phi$ ) increase with  $x$ .

### ACKNOWLEDGMENTS

This work was supported by the Natural Sciences and Engineering Research Council of Canada and Lakehead University, Ontario, Canada.

Doctors Patrick Woodward, Jeffrey Foley, and Andrew McDonald and two reviewers for the *Journal of Solid State Chemistry* provided many constructive comments on the early version of the manuscript and on use of conventional and unconventional settings in the monoclinic system. Dr. J. Rodriguez-Carvajal is thanked for providing access to the FULLPROF program.

### REFERENCES

1. A. R. Chakhmouradian and R. H. Mitchell, *Can. Mineral.* **35**, 1293 (1997).
2. R. H. Mitchell, J. B. Choi, F. C. Hawthorne, C. A. McCammon, and P. C. Burns, *Can. Mineral.* **35**, in press (1997).
3. St. v. Náráy-Szabó, *Naturwissenschaften* **41**, 202 (1943).
4. H. F. Kay and P. C. Bailey, *Acta Crystallogr.* **10**, 219 (1957).
5. S. Sasaki, C. T. Prewitt, J. D. Bass, and W. A. Schulze, *Acta Crystallogr. Sect. C* **43**, 1668 (1987).
6. R. H. Buttner and E. N. Maslen, *Acta Crystallogr. Sect. B* **48**, 644 (1992).
7. X. Liu and R. C. Liebermann, *Phys. Chem. Miner.* **20**, 171 (1993).
8. A. Beran, E. Libowitzky, and T. Armbruster, *Can. Mineral.* **34**, 803 (1996).
9. A. V. Arakcheeva, D. Yu. Pushcharovskii, V. M. Gekimiyants, V. A. Popov, and G. U. Lubman, *Kristallografiya* **42**, 54 (1997). [In Russian]
10. A. M. Glazer, *Acta Crystallogr. Sect. B* **28**, 3384 (1972).
11. V. S. Filip'ev and E. G. Fesenko, *Sov. Phys. Crystallogr.* **10**, 243 (1965).
12. E. G. Fesenko, V. S. Filip'ev, and M. F. Kupriyanov, *Izv. Akad. Nauk. SSSR Ser. Fiz.* **28**, 669 (1964). [In Russian]
13. H. Brusset, H. Gillier-Pandraud, and M. Pax Rajaonera, *C. R. Seances Acad. Sci. Ser. C* **271**, 810 (1970).
14. P. M. Woodward, R.-D. Hoffman, and A. W. Sleight *J. Mater. Res.* **9**, 2118 (1994).
15. P. M. Woodward, Ph.D. Thesis. Oregon State University, 1996.
16. R. D. Shannon, *Acta Crystallogr. Sect. A* **32**, 751 (1976).
17. J. Rodriguez-Carvajal, "FULLPROF program: Rietveld Pattern Matching Analysis of Powder Patterns." Institut Leue-Longevin, Grenoble, 1990.
18. R. H. Mitchell and N. V. Vladykin, *Mineral. Mag.* **57**, 651 (1993).
19. Yu. Zhao, D. J. Weidner, J. B. Parise, and D. E. Cox, *Phys. Earth Planet. Inter.* **76**, 1 (1993).
20. H. D. Megaw, "Crystal Structures: A Working Approach." Saunders, Philadelphia, 1973.
21. W. A. Groen, F. P. F. van Berkel, and D. J. W. Ijdo, *Acta Crystallogr. Sect. C* **42**, 1472 (1986).
22. M. T. Anderson, K. B. Greenwood, G. A. Taylor, and K. R. Poeppelmeier, *Prog. Solid State Chem.* **22**, 197 (1993).
23. P. M. Woodward, *Acta Crystallogr. Sect. B* **53**, 32 (1997).
24. S. Nomura and T. Nakagawa, *J. Phys. Soc. Jpn.* **30**, 491 (1971).